

Article

Improving the Robustness of Entangled States by Basis Transformation

Xin-Wen Wang ^{1,2,3,*}, Shi-Qing Tang ^{1,2,3}, Yan Liu ^{1,2} and Ji-Bing Yuan ^{1,2}

¹ College of Physics and Electronic Engineering, Hengyang Normal University, Hengyang 421002, China; sqtang@hynu.edu.cn (S.-Q.T.); liuyan@hynu.edu.cn (Y.L.); jbyuan@hynu.edu.cn (J.-B.Y.)

² Hunan Provincial Key Laboratory of Intelligent Information Processing and Application, Hengyang Normal University, Hengyang 421002, China

³ Key Laboratory of Low-Dimensional Quantum Structures and Quantum Control of Ministry of Education, Hunan Normal University, Changsha 410081, China

* Correspondence: xwwang@hynu.edu.cn

Received: 28 November 2018; Accepted: 7 January 2019; Published: 13 January 2019



Abstract: In the practical application of quantum entanglement, entangled particles usually need to be distributed to many distant parties or stored in different quantum memories. In these processes, entangled particles unavoidably interact with their surrounding environments, respectively. We here systematically investigate the entanglement-decay laws of cat-like states under independent Pauli noises with unbalanced probability distribution of three kinds of errors. We show that the robustness of cat-like entangled states is not only related to the overall noise strength and error distribution parameters, but also to the basis of qubits. Moreover, we find that whether a multi-qubit state is more robust in the computational basis or transversal basis depends on the initial entanglement and number of qubits of the state as well as the overall noise strength and error distribution parameters of the environment. However, which qubit basis is conducive to enhancing the robustness of two-qubit states is only dependent on the error distribution parameters. These results imply that one could improve the intrinsic robustness of entangled states by simply transforming the qubit basis at the right moment. This robustness-improving method does not introduce extra particles and works in a deterministic manner.

Keywords: entanglement robustness; cat-like states; local Pauli noises; robustness-enhancement method; basis transformation

1. Introduction

Quantum entanglement, a typical non-classical correlation between quantum systems, is at the center of quantum information science [1–4]. Most quantum communication, computation, and metrology protocols are based on quantum entanglement [5–7]. However, entanglement is very fragile due to the unavoidable interactions between the entangled systems and their surrounding environments [8]. Local system–environment interaction usually happens in the scenarios related to quantum communication and distributed quantum computation where entangled particles are far apart [9,10]. Entanglement decay, resulting from environment-induced decoherence, will negatively affect the quality of related quantum information processing tasks [10–12]. The problem on how to harness entanglement of quantum systems against the detrimental effects of the environment is of utmost importance within the vast domain of studies of quantum entanglement, since it is directly connected to the applications of quantum entanglement [13,14]. A variety of strategies have been proposed for protecting quantum entanglement [15–33].

Entanglement distillation is a prevalent way to improve the entanglement of distant particles in mixed states [33–36]. Except for some special scenarios [37–39], the initial fidelity (relative

to maximally entangled states) or entanglement degree of the source states (input states) in an entanglement distillation protocol must be larger than a threshold [33–36]. Generally, the higher degree of entanglement the input states have, the higher degree of entanglement the output states have, or the higher the distillation efficiency is, provided that the initial entanglement of the source states meets the threshold requirement. Quantum filtration methods could be used to probabilistically increase the fidelity of source states with particular structures such that it meets the threshold required for an entanglement distillation protocol [40,41]. However, quantum filtering operations may decrease the final distillation efficiency in the case where the entanglement degree of the source states exceeds the required threshold [42]. Enhancing the intrinsic robustness of entangled states is thus of importance [43–47].

Pauli noise is a kind of typical noise for qubits [8,9]. The action of a general Pauli noise on any state ρ of a qubit can be formulated as

$$\mathcal{E}(\rho) = \left(1 - \frac{p}{2}\right) \rho + \frac{p}{2} (a_x \sigma_x \rho \sigma_x + a_y \sigma_y \rho \sigma_y + a_z \sigma_z \rho \sigma_z), \quad (1)$$

where σ_x , σ_y , and σ_z are the conventional three Pauli matrices in the computational basis $\{|0\rangle, |1\rangle\}$. Parameters $0 \leq a_x, a_y, a_z \leq 1$ satisfy the normalization condition $a_x + a_y + a_z = 1$. Probability $0 \leq p \leq 1$ measures the noise strength and gives also a convenient parametrization of time: $p = 0$ refers to the initial time $t = 0$ and $p = 1$ refers to the asymptotic $t \rightarrow \infty$ limit. Note that the $1/2$ factors in Equation (1) are such that an exact fully dephasing channel appears at $p = 1$ and $a_z = 1$. The particular examples of single-qubit Pauli noises are the depolarizing, phase-flip, bit-flip, and bit-phase-flip channels, which correspond to $a_x = a_y = a_z = 1/3$, $a_z = 1$ ($a_x = a_y = 0$), $a_x = 1$ ($a_y = a_z = 0$), and $a_y = 1$ ($a_x = a_z = 0$), respectively. A depolarizing channel describes that the qubit is subjected to bit-flip (σ_x), phase-flip (σ_z), and bit-phase-flip (σ_y) errors with the same probability. In the other three noise channels, only one type of error happens. An entangled state usually displays different robustness in different noise channels [48–51]. The robustness of different entangled states, even with the same initial entanglement, may be different in the same noise channel [44,47,52].

In many cases, the above-mentioned three types of errors may happen with different probabilities [12,47]. Two examples are listed below. Consider that several physical qubits are used to encode one logical qubit. Errors acting on the individual qubits lead to the populations outside the logical subspace. However, active quantum error correction allows one to correct certain errors, while other errors may lead to an error at the logical level. It has been shown that, for a repetition code capable of correcting bit-flip errors, depolarizing noise at the physical level leads to effective Pauli noise with a preferred direction at the logical level [53]. Generally, depolarizing noise acting on physical qubits encoding a logical qubit could be modeled as effective Pauli noise, with unbalanced probability distribution for the three errors, acting on the logical qubit [53]. Another example is provided by thermal baths with infinite temperature, where the decoherence of a qubit can be described by a Pauli map with $a_x = a_y \neq a_z$ [12,44].

In this paper, we investigate the disentanglement features and robustness of n -qubit ($n \geq 2$) cat-like entangled states under the local (independent) Pauli channels where the probabilities of three kinds of errors occurring are not the same. We mainly discuss three issues. One is how the error distribution parameters (a_x, a_y, a_z) affect the residual entanglement. Another one is whether the initial entanglement degree of an entangled state has influence on its decay law. The third one is how the qubit basis impacts the entanglement-robustness of cat-like states. What we are most interested in is under which qubit basis (computational or transversal basis) an entangled state is more robust in a noisy environment. We shall show that the answer depends not only on the noise parameters, but also on the entanglement degree of the original entangled state and the number of involved qubits. More interestingly, two-qubit entangled states may exhibit the opposite phenomenon to multi-qubit entangled states.

2. Robustness of Cat-Like States and Its Enhancement Method

When n Pauli noises independently act on n qubits of any state ρ , the composite n -qubit map \mathcal{M} is given by the single-qubit map composition

$$\mathcal{M}(\rho) = \mathcal{E}_1 \otimes \mathcal{E}_2 \otimes \cdots \mathcal{E}_k \otimes \cdots \mathcal{E}_n(\rho), \tag{2}$$

where \mathcal{E}_k , with $1 \leq k \leq n$, corresponds to map (1) acting on the k th qubit. We shall discuss the entanglement-robustness of different n -qubit cat-like states under the map \mathcal{M} . The entanglement between any two parts of a decohered state, e.g., one qubit versus the rest, will be measured by the negativity [54,55]. Following Ref. [55], the negativity can be defined as

$$\mathcal{N}(\rho) = -2\lambda_{\min}, \tag{3}$$

where λ_{\min} is the sum of all minus eigenvalues of the partial transpose of the state ρ . Note that, when the two parts are separable, one should let $\lambda_{\min} \equiv 0$. It will be shown that the robustness of an entangled state is dependent on the form of qubit basis, the number of qubits n , the noise strength p , and the error distribution parameters (a_x, a_y, a_z) . Moreover, two-qubit entangled states express different decoherence behaviours from multi-qubit entangled states.

2.1. Robustness of Cat-Like States in the Computational Basis

For the initial n -qubit ($n \geq 2$) cat-like states

$$|\Phi_n^+\rangle = \alpha|0\rangle^{\otimes n} + \beta|1\rangle^{\otimes n} \tag{4}$$

with $\alpha^2 + \beta^2 = 1$ (for simplicity, α and β are assumed to be real), the amount of entanglement between any two partitions is

$$\mathcal{N}_i = 2|\alpha\beta|. \tag{5}$$

When $|\alpha| = |\beta| = 1/\sqrt{2}$, $\mathcal{N}_i = 1$ and the n -qubit states in Equation (4) are maximally entangled states. If $|\alpha| \neq |\beta|$, $\mathcal{N}_i < 1$ and these states are partially entangled pure states. The decohered states $\mathcal{M}(|\Phi_n^+\rangle)$ are X states [46,56]. For any bipartition of an n -qubit X matrix, its partial-transpose is still an X matrix with the same dimension. Calculation of the eigenvalues of a $2^n \times 2^n$ -dimensional X matrix is essentially equivalent to diagonalizing 2^{n-1} matrices of dimension 2×2 . With these features, one can calculate, in a straightforward way, the negativity \mathcal{N} of any bipartition “one qubit versus the rest” of $\mathcal{M}(|\Phi_n^+\rangle)$.

For the phase-flip channel \mathcal{M}^{PF} , i.e., $a_z = 1$, we have

$$\mathcal{N}_{(a_z=1)} = (1 - p)^n \mathcal{N}_i. \tag{6}$$

Obviously, $\mathcal{N}_{(a_z=1)}$ decays exponentially with n , as $(1 - p)^n$. In fact, all the entanglement in the state $|\Phi_n^+\rangle$ under \mathcal{M}^{PF} decays (at slowest) exponentially with n . This implies that the state $|\Phi_n^+\rangle$ is very fragile to the phase-flip noise.

As to a non-pure phase-damping channel, i.e., $a_z < 1$, the negativity of any bipartition “one qubit versus the rest” of $\mathcal{M}(|\Phi_n^+\rangle)$ can also be analytically calculated, which is given by (Appendix A)

$$\mathcal{N} = \sum_{u=0}^{\lfloor \frac{n-1}{2} \rfloor} \binom{n-1}{u} [\max(0, G_u - F_{u+1}) + \max(0, H_u - F_u)], \tag{7}$$

where $\lfloor \frac{n-1}{2} \rfloor = (n - 1)/2$, for n being odd, or $\lfloor \frac{n-1}{2} \rfloor = n/2 - 1$, for n being even, and

$$F_u = A^{n-u}B^u + A^uB^{n-u}, \tag{8}$$

$$G_u = \left[\left(A^{n-u-1}B^{u+1} - A^{u+1}B^{n-u-1} \right)^2 \left(1 - \mathcal{N}_i^2 \right) + \left(C^{n-u}D^u + C^u D^{n-u} \right)^2 \mathcal{N}_i^2 \right]^{1/2}, \tag{9}$$

$$H_u = \left[\left(A^{n-u}B^u - A^uB^{n-u} \right)^2 \left(1 - \mathcal{N}_i^2 \right) + \left(C^{n-u-1}D^{u+1} + C^{u+1}D^{n-u-1} \right)^2 \mathcal{N}_i^2 \right]^{1/2}, \tag{10}$$

$$A = 1 - \frac{p}{2} + \frac{p}{2}a_z, \tag{11}$$

$$B = \frac{p}{2}a_x + \frac{p}{2}a_y, \tag{12}$$

$$C = 1 - \frac{p}{2} - \frac{p}{2}a_z, \tag{13}$$

$$D = \frac{p}{2}a_x - \frac{p}{2}a_y. \tag{14}$$

Obviously, the negativity of the decohered state is dependent on both channel parameters (a_x, a_y, a_z, p) and the amount of entanglement of the initial state (\mathcal{N}_i) . In the following, we shall show some interesting results.

We first discuss the case $\mathcal{N}_i = 1$, i.e., the original state in Equation (4) is a standard Greenberger–Horne–Zeilinger (GHZ) state ($n \geq 3$) or Bell state ($n = 2$). When the initial state is a standard GHZ, the variation tendency of negativity \mathcal{N} of the decohered state with error distribution parameters (a_x, a_y, a_z) is related to the overall noise strength p . For a given a_y , the increase (decrease) in a_x will always lead to increase (decrease) in the negativity \mathcal{N} when p is small; however, \mathcal{N} may first slowly decrease and then increase (even rapidly) with the increase of a_x when p exceeds a threshold (see, e.g., Figure 1). It can be seen from Figure 1 that the threshold of p is usually related to n , and the larger n , the smaller threshold, and that, for a given n , the larger p is, the larger a_x the knee point of \mathcal{N} happens at. Moreover, the larger n is, \mathcal{N} is more dependent on a_x , i.e., it is more sensitive to the change of a_x . Overall, for given p and a_y , the residual entanglement of the decohered GHZ state tends to a maximum when $a_x \rightarrow 1 - a_y$. These phenomena imply that the standard GHZ states under the computational basis are the most robust against the noise of σ_x direction (which is vertical to the qubit-basis direction in the Bloch sphere), and that the variation tendency of the negativity of a decohered state with the weight of the σ_x -directional noise is slightly modulated by the overall noise strength.

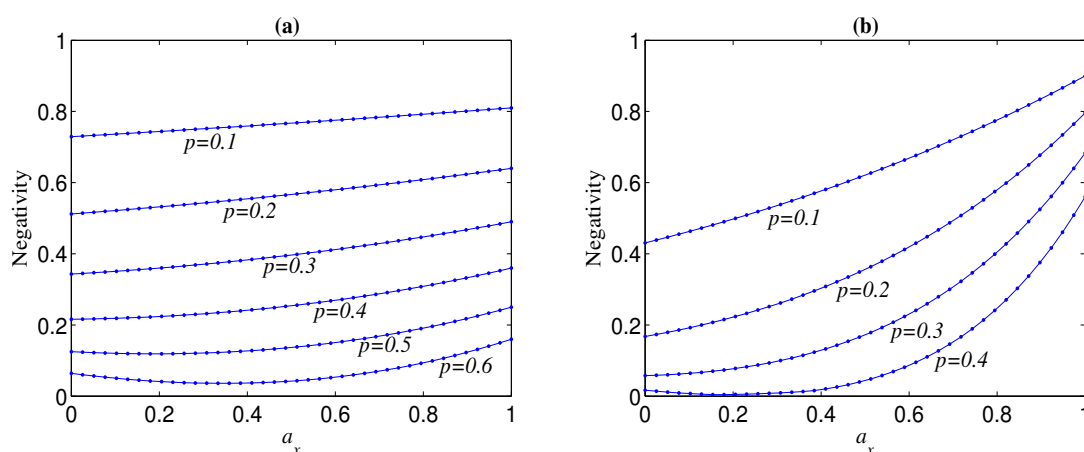


Figure 1. Negativity of decohered state $\mathcal{M}(|\Phi_n^+\rangle)$, as a function of a_x , for different noise strength p , where $a_y = 0$ and $\mathcal{N}_i = 1$. (a) $n = 3$; (b) $n = 8$.

The Bell state displays different decoherence behaviour from GHZ states. For any given p and a_y , $\mathcal{N}_{(n=2)}$ is not monotonous with a_x and the knee point always happens at $a_x = (1 - a_y)/2$, though a_x

has a very slight influence on it (see, e.g., Figure 2). Furthermore, $\mathcal{N}_{(n=2)}$ takes a maximum when a_x equals to zero or $1 - a_y$. In other words, when $a_x < (1 - a_y)/2$ ($a_x > (1 - a_y)/2$), the smaller (larger) a_x , the larger $\mathcal{N}_{(n=2)}$. These results indicate that when the weights of the phase-flip error and bit-flip error are more different, the Bell state is more robust.

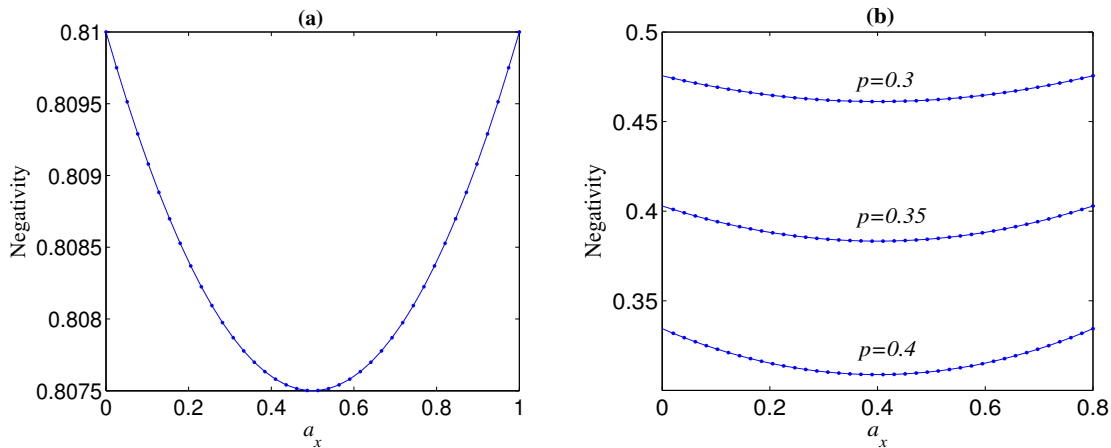


Figure 2. Negativity of decohered state $\mathcal{M}(|\Phi_2^+\rangle)$, as a function of a_x , for different noise strength p , where $\mathcal{N}_i = 1$. (a) $a_y = 0$, $p = 0.1$; (b) $a_y = 0.2$.

One can check another interesting phenomenon that a_y has a similar influence with a_x on \mathcal{N} (see, e.g., Figure 3). This phenomenon could be partly understood from the fact that both eigenvectors of noisy operators σ_y and σ_x are vertical to basis vectors $|0\rangle$ and $|1\rangle$ in the Bloch sphere. Moreover, for any given a_z , \mathcal{N} always takes a minimum when $a_y = (1 - a_z)/2$, i.e., $a_y = a_x$ (see Figure 3). This conclusion can be directly obtained from Equation (7) when $n = 2$. As to $n > 2$, it could be explained as follows. The standard GHZ states under the computational basis are the most fragile to the phase-flip error and the most robust against the bit-flip error (will be shown later). On the other hand, the noisy operator σ_y has both phase-flip and bit-flip actions. Thus, there is a trade-off between the negative effect and positive effect of the weight of the phase-bit-flip error. For a given a_z , the relation between \mathcal{N} and a_y is clearly shown in Figure 4. It can be seen from Figure 4 that the influence degree of a_y on \mathcal{N} is symmetric about $a_y = (1 - a_z)/2$ for both Bell and GHZ states, and \mathcal{N} takes a maximum when a_y equals to zero or $1 - a_z$.

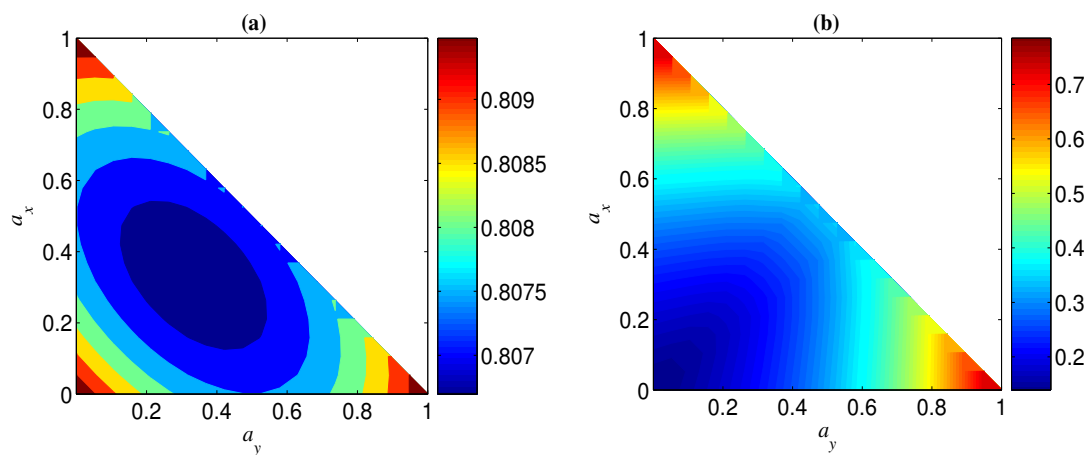


Figure 3. Negativity as a function of a_x and a_y for initial maximally entangled pure state $|\Phi_n^+\rangle$ under local decoherence. (a) $n = 2$, $p = 0.1$; (b) $n = 9$, $p = 0.2$.

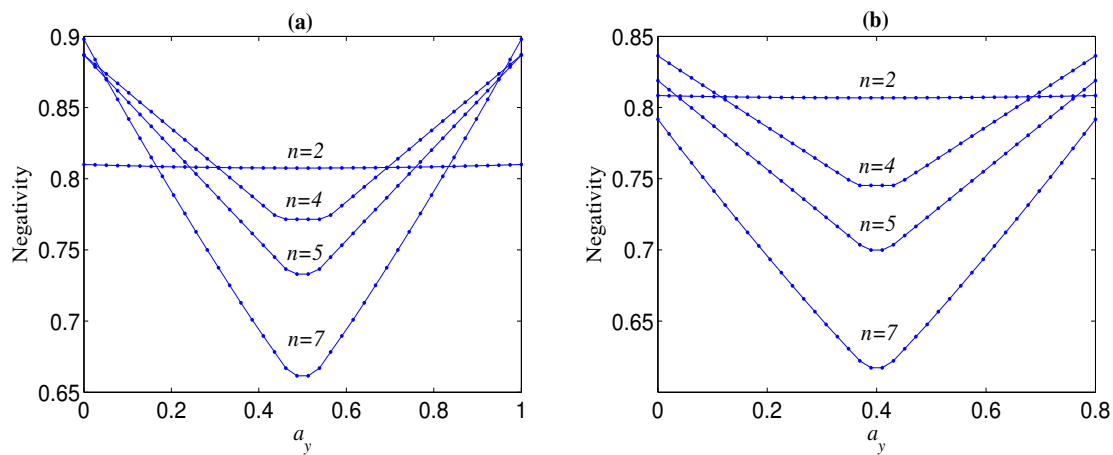


Figure 4. Negativities as functions of a_y for different initial pure states $|\Phi_n^+\rangle$ with $\mathcal{N}_i = 1$ under local decoherence, where $p = 0.1$. (a) $a_z = 0$; (b) $a_z = 0.2$.

The influence of the channel parameters on the negativity \mathcal{N} of the decohered state is also relative to the amount of entanglement \mathcal{N}_i of the initial state (4). As examples, Figures 5 and 6 show that, when $\mathcal{N}_i < 1$ (i.e., $|\alpha| \neq |\beta|$), \mathcal{N} (for a given a_y) exhibits different dynamic behaviour with the variation of a_x from the case $\mathcal{N}_i = 1$ (i.e., $|\alpha| = |\beta|$) for $n = 2, 3$, respectively. Specifically, if $\mathcal{N}_i < 1$, $\mathcal{N}_{(n=2)}$ tends to a minimum when $a_x \rightarrow 1 - a_y$ (e.g., $a_y = 0$), in contrast to the case $\mathcal{N}_i = 1$ where $\mathcal{N}_{(n=2)}$ tends to a maximum when $a_x \rightarrow 1 - a_y$. In the case $\mathcal{N}_i < 1$ (e.g., $\mathcal{N}_i = 0.6$), $\mathcal{N}_{(n=3)}$ takes a maximum at $a_x = 0$ when p exceeds a threshold. One can check that, for $\mathcal{N}_i < 1$, $\mathcal{N}_{(n \geq 4)}$ could also take a maximum at $a_x = 0$ when p is very large. Note that, if $\mathcal{N}_i = 1$, \mathcal{N} always reaches a maximum when a_x increases to $1 - a_y$ for any given p and a_y , as mentioned above. The difference of the decay behaviours of partially entangled states and maximally ones may be partly understood from the fact that the two distinguishable product states $(|0\rangle^{\otimes n}$ and $|1\rangle^{\otimes n})$ are superposed with unequal weights in the former and equal weight in the latter.

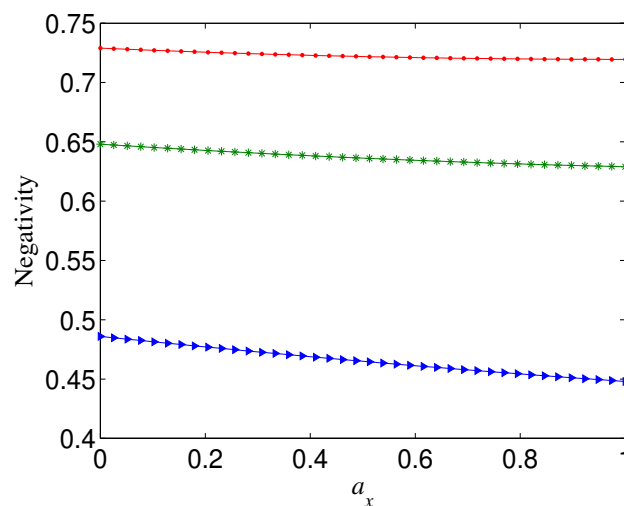


Figure 5. Negativity of decohered state $\mathcal{M}(|\Phi_2^+\rangle)$, as a function of a_x , for $\mathcal{N}_i = 0.9$ (red dots), 0.8 (green stars), or 0.6 (blue triangles), where $a_y = 0$, $p = 0.1$.

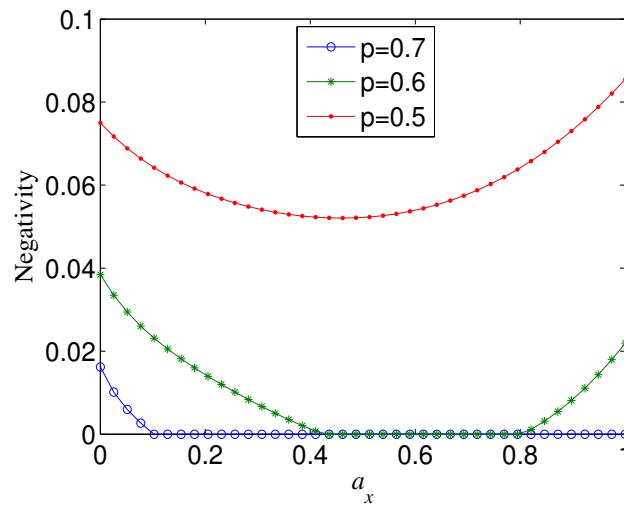


Figure 6. Negativity of decohered state $\mathcal{M}(|\Phi_3^+\rangle)$ versus noisy parameter a_x , where $a_y = 0$, $\mathcal{N}_i = 0.6$.

From Figure 4a, we can also observe that the more larger n , \mathcal{N} is more sensitive to the change of a_y (or a_x), which leads to the fact that when a_y tends to zero (a_y tends to one) and a_x tends to one (a_x tends to zero), $\mathcal{N}_{(n=M)}$ could be larger than $\mathcal{N}_{(n=L)}$ with $M > L \geq 2$. Figure 7 shows the trend of the negativity \mathcal{N} with the variation of number of qubits n when a_y is near to zero (a_y is near to one) and a_x is near to one (a_x is near to zero). It can be seen from Figure 7 that the total variation tendency of \mathcal{N} with n is independent from the initial entanglement \mathcal{N}_i . Figure 7 also implies that the optimal n that maximizes the bipartite entanglement of the decohered n -qubit state is dependent on a_x (a_y) when $a_y \rightarrow 0$ ($a_x \rightarrow 0$). In Figure 8, we give the aforementioned optimal n for different a_x with $a_y = 0$. From Figure 8, we can deduce that, when a_x is infinitely close to one, the optimal n always tends to infinity.

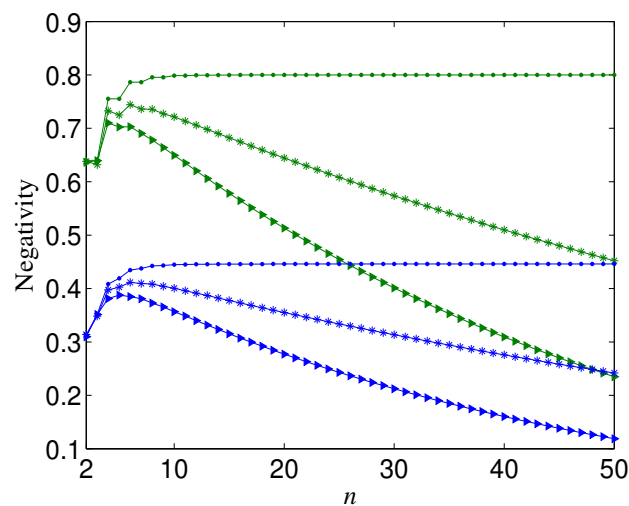


Figure 7. Negativity (\mathcal{N}) versus n , where $p = 0.2$. Green lines correspond to $\mathcal{N}_i = 1$; blue lines correspond to $\mathcal{N}_i = 0.6$. Dots correspond to $a_x = 1$, $a_y = 0$; stars correspond to $a_x = 0.95$, $a_y = 0$; triangles correspond to $a_x = 0.9$, $a_y = 0.1$.

In fact, when $a_x = 1$, the channel map \mathcal{M} reduces to the bit-flip channel \mathcal{M}^{BF} , and we can analytically obtain

$$E\left(\mathcal{M}^{\text{BF}}(|\Phi_n^+\rangle)\right) \geq E\left(\mathcal{M}^{\text{BF}}(|\Phi_{n-1}^+\rangle)\right) \geq \dots \geq E\left(\mathcal{M}^{\text{BF}}(|\Phi_2^+\rangle)\right), \tag{15}$$

where $E(\cdot)$ is an arbitrary entanglement measure. Note that this result is independent from the noise strength p . It can be understood as follows. A single-qubit σ_x measurement on $|\Phi_n^+\rangle$ leaves the system in state $|\Phi_{n-1}^+\rangle \otimes |+\rangle$ or $|\Phi_{n-1}^-\rangle \otimes |-\rangle$, with $|\pm\rangle = (|0\rangle + |1\rangle)/\sqrt{2}$ being the eigenstates of σ_x and $|\Phi_{n-1}^-\rangle = \alpha|0\rangle^{\otimes n-1} - \beta|1\rangle^{\otimes n-1}$. Similarly, since it commutes with \mathcal{M}^{BF} , a σ_x measurement on $\rho_n^+ = \mathcal{M}^{\text{BF}}(|\Phi_n^+\rangle)$ leaves the system in $\rho_{n-1}^+ \otimes |+\rangle\langle +|$ or $\rho_{n-1}^- \otimes |-\rangle\langle -|$, with $\rho_{n-1}^- = \mathcal{M}^{\text{BF}}(|\Phi_{n-1}^-\rangle)$. Furthermore, it is immediate to see that $\rho_{n-1}^+ \otimes |+\rangle\langle +|$ and $\rho_{n-1}^- \otimes |-\rangle\langle -|$ are local-unitarily equivalent. Thus, we can say $E(\rho_n^+) \geq E(\rho_{n-1}^+)$. Iterating this reasoning $n - 2$ times and, for ease of notation, omitting the tensor-product factors, one can obtain Equation (15). For specific calculation of the negativity given in Equation (7), one can omit the second term in each square bracket because H_u is impossible to be larger than F_u when $a_x = 1$.

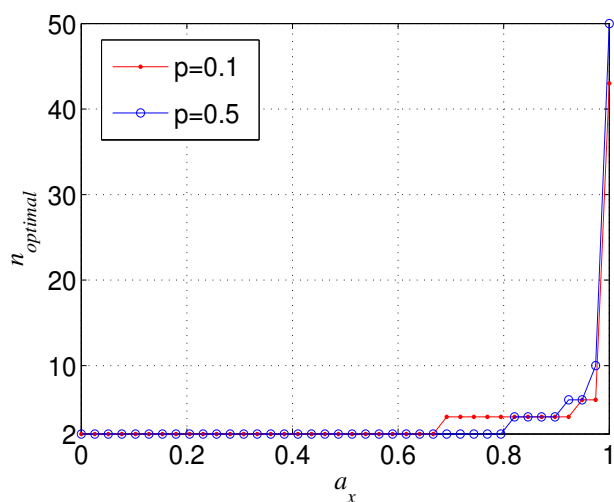


Figure 8. The optimal n ($n_{optimal}$) that maximizes \mathcal{N} for different a_x , where $\mathcal{N}_i = 1$ and $a_y = 0$.

2.2. Robustness of Cat-Like States in the Transversal Basis

By local Hadamard-gate rotation $\mathcal{H} = |+\rangle\langle 0| + |-\rangle\langle 1|$, the cat-like state $|\Phi_n^+\rangle$ can be transformed into the transversal form, i.e.,

$$|\Phi_n^{+T}\rangle = \mathcal{H}^{\otimes n}|\Phi_n^+\rangle = \alpha|+\rangle^{\otimes n} + \beta|-\rangle^{\otimes n}. \tag{16}$$

The transversal state $|\Phi_n^{+T}\rangle$ is local-unitarily equivalent to $|\Phi_n^+\rangle$, and thus possesses the same amount and type of entanglement as $|\Phi_n^+\rangle$. However, it will be shown that $|\Phi_n^{+T}\rangle$ may display a very different decoherence behaviour from $|\Phi_n^+\rangle$ in the same noisy environment.

The decohered state $\mathcal{M}(|\Phi_n^{+T}\rangle)$ is also an X state under the transversal qubit-basis $\{|+\rangle, |-\rangle\}$. In the local bit-flip channels, i.e., $a_x = 1$, the negativity \mathcal{N}^T of any bipartition “one qubit versus the rest” of $\mathcal{M}(|\Phi_n^{+T}\rangle)$ is the same as $\mathcal{N}_{(a_x=1)}$ in Equation (6). For $a_x < 1$, \mathcal{N}^T has the same form as Equation (7), but with A, B, C, D being replaced, respectively, by A', B', C', D' , which are given by

$$A' = 1 - \frac{p}{2} + \frac{p}{2}a_x, \tag{17}$$

$$B' = \frac{p}{2}a_z + \frac{p}{2}a_y, \tag{18}$$

$$C' = 1 - \frac{p}{2} - \frac{p}{2}a_x, \tag{19}$$

$$D' = \frac{p}{2}a_z - \frac{p}{2}a_y. \tag{20}$$

The dependency relationship of \mathcal{N}^T on a_x (a_z) is different from that of \mathcal{N} on a_x (a_z). If $a_z = 1$, the Pauli channel \mathcal{M} reduces to the phase-flip channel \mathcal{M}^{PF} , the inequalities in Equation (15) also hold for states $\mathcal{M}^{PF}(|\Phi_n^{+T}\rangle)$. As a matter of fact, the role of a_z in \mathcal{N}^T is the same as that of a_x in \mathcal{N} . The essential cause is that the action of operator σ_z on the basis states $\{|+\rangle, |-\rangle\}$ is the same as σ_x on $\{|0\rangle, |1\rangle\}$, and vice versa. Thus, the result about the influence of a_x on the residual entanglement of $|\Phi_n^+\rangle$ in the noisy environment described by \mathcal{M} shown in the former subsection is also applicable for the influence of a_z on the residual entanglement of $|\Phi_n^{+T}\rangle$.

The impact of a_y on both $\mathcal{M}(|\Phi_n^{+T}\rangle)$ and $\mathcal{M}(|\Phi_n^+\rangle)$ is the same. This is due to the fact that $\sigma_y|0\rangle\langle 0|\sigma_y = \sigma_y|+\rangle\langle +|\sigma_y, \sigma_y|1\rangle\langle 1|\sigma_y = \sigma_y|-\rangle\langle -|\sigma_y$, and $\sigma_y|0\rangle\langle 1|\sigma_y = \sigma_y|+\rangle\langle -|\sigma_y$, that is, the operator σ_y has the same effect on a qubit under both bases. If $a_y = 1$, i.e., the channel \mathcal{M} reduces to the bit-phase-flip channel \mathcal{M}^{BPF} , the inequalities in Equation (15) hold for both states $\mathcal{M}^{BPF}(|\Phi_n^+\rangle)$ and $\mathcal{M}^{BPF}(|\Phi_n^{+T}\rangle)$. It can be understood as follows. A single-qubit σ_y measurement on $|\Phi_n^+\rangle$ leaves the system in state $|\Phi_{n-1}'^-\rangle \otimes |+\rangle_y$ or $|\Phi_{n-1}'^+\rangle \otimes |-\rangle_y$, with $|\pm\rangle_y = (|0\rangle \pm i|1\rangle)/\sqrt{2}$ being the eigenstates of σ_y and $|\Phi_{n-1}'^\pm\rangle = \alpha|0\rangle^{\otimes n-1} \pm i\beta|1\rangle^{\otimes n-1}$. Note that $|\Phi_{n-1}'^\pm\rangle$ are local-unitarily equivalent to $|\Phi_{n-1}^\pm\rangle$. Similarly, since it commutes with \mathcal{M}^{BPF} , a σ_y measurement on $\rho_n^+ = \mathcal{M}^{BPF}(|\Phi_n^+\rangle)$ leaves the system in $\rho_{n-1}'^- \otimes |+\rangle_y\langle +|$ or $\rho_{n-1}'^+ \otimes |-\rangle_y\langle -|$, with $\rho_{n-1}'^\pm = \mathcal{M}^{BPF}(|\Phi_{n-1}'^\pm\rangle)$. Furthermore, it is immediate to see that $\rho_{n-1}'^\pm$ are local-unitarily equivalent to ρ_{n-1}^\pm . Thus, we can say $E(\rho_n^+) \geq E(\rho_{n-1}^+)$. Iterating this reasoning $n - 2$ times and, for ease of notation, omitting the tensor-product factors, one can obtain Equation (15) for states $\mathcal{M}^{BPF}(|\Phi_n^+\rangle)$. In the same vein, we can also prove the inequalities in (15) for states $\mathcal{M}^{BPF}(|\Phi_n^{+T}\rangle)$. Specifically, a single-qubit σ_y measurement on $|\Phi_n^{+T}\rangle$ will leave the system in state $|\Phi_{n-1}'^{+T}\rangle \otimes |+\rangle_y$ or $|\Phi_{n-1}'^{-T}\rangle \otimes |-\rangle_y$, with $|\Phi_{n-1}'^{\pm T}\rangle = e^{\mp\pi i/4}\alpha|+\rangle^{\otimes n-1} + e^{\pm\pi i/4}\beta|-\rangle^{\otimes n-1}$ being local-unitarily equivalent to $|\Phi_{n-1}^{+T}\rangle$. Then, a σ_y measurement on $\rho_n^{+T} = \mathcal{M}^{BPF}(|\Phi_n^{+T}\rangle)$ will leave the system in $\rho_{n-1}'^{+T} \otimes |+\rangle_y\langle +|$ or $\rho_{n-1}'^{-T} \otimes |-\rangle_y\langle -|$, with $\rho_{n-1}'^{\pm T} = \mathcal{M}^{BPF}(|\Phi_{n-1}'^{\pm T}\rangle)$ being local-unitarily equivalent to ρ_{n-1}^{+T} . Thus, we can conclude $E(\rho_n^{+T}) \geq E(\rho_{n-1}^{+T})$. Repeating the process above $n - 2$ times, one can verify Equation (15) for states $\mathcal{M}^{BPF}(|\Phi_n^{+T}\rangle)$.

It should be pointed out again that σ_y plays the same role as σ_x in states $\mathcal{M}(|\Phi_n^+\rangle)$ (see Figures 3 and 4) and as σ_z in states $\mathcal{M}(|\Phi_n^{+T}\rangle)$. This may be partly understood from the fact that the eigenvectors of both noisy operators σ_y and σ_x are transversal to the qubit basis $\{|0\rangle, |1\rangle\}$, and the eigenvectors of both σ_y and σ_z are transversal to the qubit basis $\{|+\rangle, |-\rangle\}$.

2.3. Enhancing the Robustness of Cat-Like States by Basis Transformation

According to the discussion above, we obtain that, under the local Pauli channels with unbalanced probability distribution for three kinds of errors, the entanglement-robustness of cat-like states are generally related to the qubit basis. This implies that one can enhance the robustness of entangled states by transforming the qubit basis according to preestimated channel features. In this subsection, we investigate in what conditions the basis $\{|0\rangle, |1\rangle\}$ is better than $\{|+\rangle, |-\rangle\}$, or otherwise. This can be achieved by comparing the negativity \mathcal{N}^T of $\mathcal{M}(|\Phi_n^{+T}\rangle)$ and the negativity \mathcal{N} of $\mathcal{M}(|\Phi_n^+\rangle)$. If the difference

$$\Delta\mathcal{N} = \mathcal{N}^T - \mathcal{N} \tag{21}$$

is larger than zero, it indicates that $|\Phi_n^{+T}\rangle$ is more robust than $|\Phi_n^+\rangle$. If $\Delta\mathcal{N} < 0$, it means $|\Phi_n^+\rangle$ is more robust than $|\Phi_n^{+T}\rangle$. As mentioned above, the noisy operator σ_y has the same effect on a qubit under

both bases $\{|+\rangle, |-\rangle\}$ and $\{|0\rangle, |1\rangle\}$; thus, $\Delta\mathcal{N} \equiv 0$ when $a_y = 1$. Then, we only need to discuss the case $a_y < 1$.

Let us begin by the phase-flip channel $a_z = 1$. For $n = 2$, it can be directly calculated that $\Delta\mathcal{N} = 0$ when $\mathcal{N}_i = 1$; however, $\Delta\mathcal{N} \leq 0$ when $\mathcal{N}_i < 1$ (see Figure 9). Thus, we can conclude that the two-qubit maximally entangled state ($|\alpha| = |\beta|$) has the same robustness under both qubit bases $\{|+\rangle, |-\rangle\}$ and $\{|0\rangle, |1\rangle\}$, but two-qubit partially entangled states ($|\alpha| \neq |\beta|$) are more robust in the basis $\{|0\rangle, |1\rangle\}$ than in the basis $\{|+\rangle, |-\rangle\}$. If consider the possible fact that it is very difficult to make $|\alpha|$ be strictly equal to $|\beta|$ in experiments, we could say that the basis $\{|0\rangle, |1\rangle\}$ is superior to the basis $\{|+\rangle, |-\rangle\}$ for two-qubit state distribution or storage.

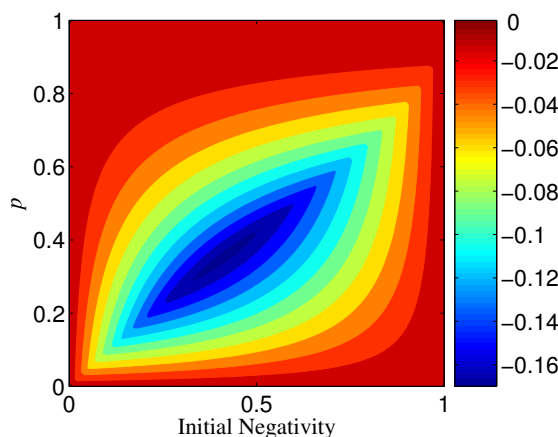


Figure 9. Variation of $\Delta\mathcal{N}$ with different p and \mathcal{N}_i when $a_z = 1$ and $n = 2$.

The results for $n \geq 3$ are not the same as that for $n = 2$. If $\mathcal{N}_i = 1$, $\Delta\mathcal{N}$ is always positive for $n \geq 3$, which indicates that the basis $\{|+\rangle, |-\rangle\}$ overmatches $\{|0\rangle, |1\rangle\}$ in keeping the entanglement of standard GHZ states. If $\mathcal{N}_i < 1$, however, the sign (positive or minus) of $\Delta\mathcal{N}$ is dependent on \mathcal{N}_i , n , and p . When \mathcal{N}_i is less than a threshold \mathcal{N}_t , $\Delta\mathcal{N} < 0$, which means that $|\Phi_n^+\rangle$ is more robust than $|\Phi_n^{+T}\rangle$ (see, e.g., Figure 10). When $\mathcal{N}_t < \mathcal{N}_i < 1$, $\Delta\mathcal{N}$ could also be minus as long as p is larger than a threshold p_t depending on \mathcal{N}_i (see Figure 10). Generally, for a given n , the larger \mathcal{N}_i , the larger p_t . In addition, the larger n , the less \mathcal{N}_t ; when n is very large, $\mathcal{N}_t \rightarrow 0$. \mathcal{N}_t with different n is given in Figure 11. We plot p_t as a function of \mathcal{N}_i and n in Figure 12.

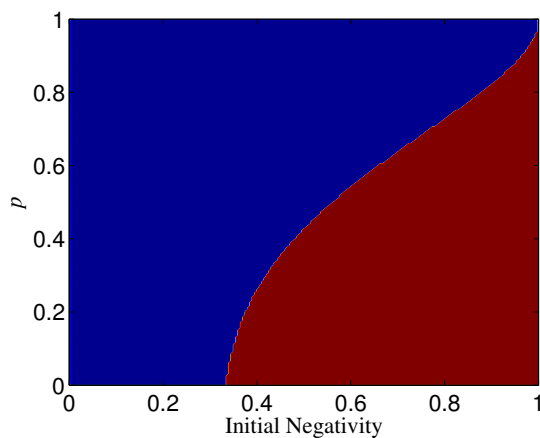


Figure 10. The sign (positive or minus) of $\Delta\mathcal{N}_{(n=3)}$ for different p and \mathcal{N}_i , where $a_z = 1$. The blue region denotes $\Delta\mathcal{N} < 0$ and the red region denotes $\Delta\mathcal{N} > 0$.

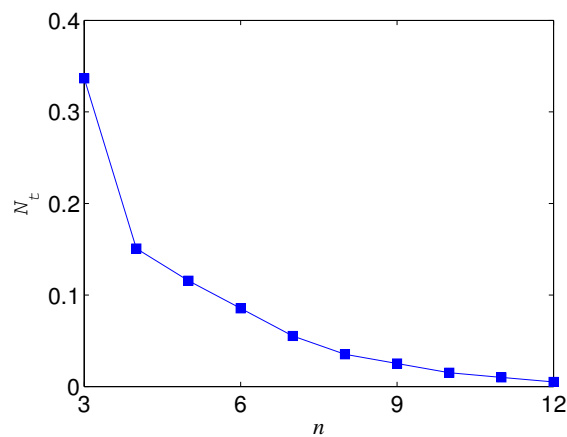


Figure 11. \mathcal{N}_t versus n , where $a_z = 1$.

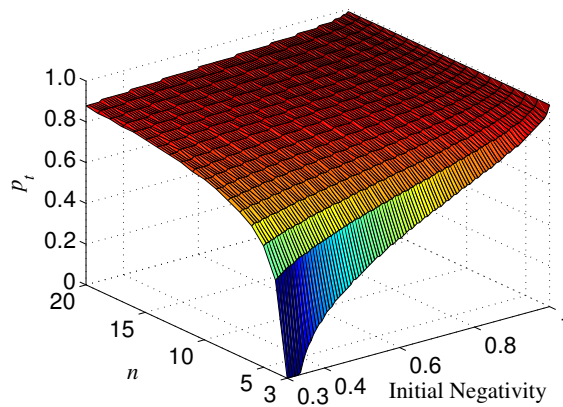


Figure 12. p_t for different \mathcal{N}_i and n , where $a_z = 1$.

As to the bit-flip channel $a_x = 1$, the results are the same as above with exchanging the roles of bases $\{|0\rangle, |1\rangle\}$ and $\{|+\rangle, |-\rangle\}$. That is, $\mathcal{N}_{(n=2)}^T \geq \mathcal{N}_{(n=2)}$ for any case, $\mathcal{N}_{(n \geq 3)}^T < \mathcal{N}_{(n \geq 3)}$ for $\mathcal{N}_i = 1$, and $\mathcal{N}_{(n \geq 3)}^T > \mathcal{N}_{(n \geq 3)}$ for $\mathcal{N}_i < \mathcal{N}_t$, or $\mathcal{N}_t < \mathcal{N}_i < 1$ but $p > p_t$.

In the case of a_z and a_x being less than one, $a_z = a_x$ is the dividing line between the two regions of $\Delta\mathcal{N} > 0$ and $\Delta\mathcal{N} < 0$ (see, e.g., Figure 13). Specifically, the region of $\Delta\mathcal{N} > 0$ can be obtained by mirroring that of $\Delta\mathcal{N} < 0$ in $a_z = a_x$ (see, e.g., Figure 13). This can be understood from the fact that the role of a_z in \mathcal{N}^T is the same as that of a_x in \mathcal{N} , as mentioned above. From Figure 13, we can also see that a_z (a_x) may have the opposite effect in $\Delta\mathcal{N}_{(n=2)}$ and $\Delta\mathcal{N}_{(n=3)}$. In other words, for given a_z and a_x , if $\Delta\mathcal{N} > 0$ for a two-qubit entangled state, $\Delta\mathcal{N} < 0$ may happen for a three-qubit entangled state. This implies that the sign of $\Delta\mathcal{N}$ is related to the number of qubits n . Moreover, the sign of $\Delta\mathcal{N}$ may also be dependent on the initial entanglement \mathcal{N}_i . We next analyze the change of the sign of $\Delta\mathcal{N}$ with a_z and \mathcal{N}_i for given p and a_y (keep in mind that $a_x = 1 - a_z - a_y$, and that the noisy operator σ_y has the same effect on a qubit under both bases $\{|+\rangle, |-\rangle\}$ and $\{|0\rangle, |1\rangle\}$). In Figure 14, we show the sign of $\Delta\mathcal{N}$ with different \mathcal{N}_i by taking $a_y = 0$ and $p = 0.1$. Figure 14a indicates that $\Delta\mathcal{N}_{(n=2)} \geq 0$ when $a_z < (1 - a_y)/2$ and $\Delta\mathcal{N}_{(n=2)} \leq 0$ when $a_z > (1 - a_y)/2$. Figure 14b, however, indicates that the sign of $\Delta\mathcal{N}_{(n=3)}$ is dependent on the value of \mathcal{N}_i for a given a_z , i.e., when \mathcal{N}_i is larger than a threshold \mathcal{N}_t , $\Delta\mathcal{N}_{(n=3)} < 0$ for $a_z < (1 - a_y)/2$ and $\Delta\mathcal{N}_{(n=3)} > 0$ for $a_z > (1 - a_y)/2$, and otherwise $\Delta\mathcal{N}_{(n=3)} > 0$ for $a_z < (1 - a_y)/2$ and $\Delta\mathcal{N}_{(n=3)} < 0$ for $a_z > (1 - a_y)/2$. Generally, the larger n is, the smaller \mathcal{N}_t is, and $\mathcal{N}_t \rightarrow 0$ when n is very large (see, e.g., Figure 15).

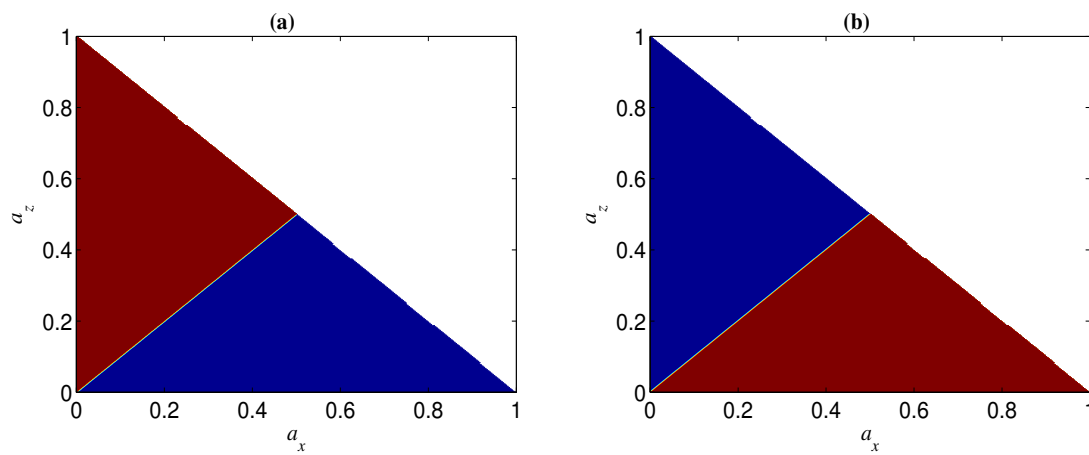


Figure 13. Regions of $\Delta\mathcal{N} < 0$ (blue) and $\Delta\mathcal{N} > 0$ (red) when $\mathcal{N}_i = 0.9$ and $p = 0.1$. (a) $n = 2$; (b) $n = 3$.

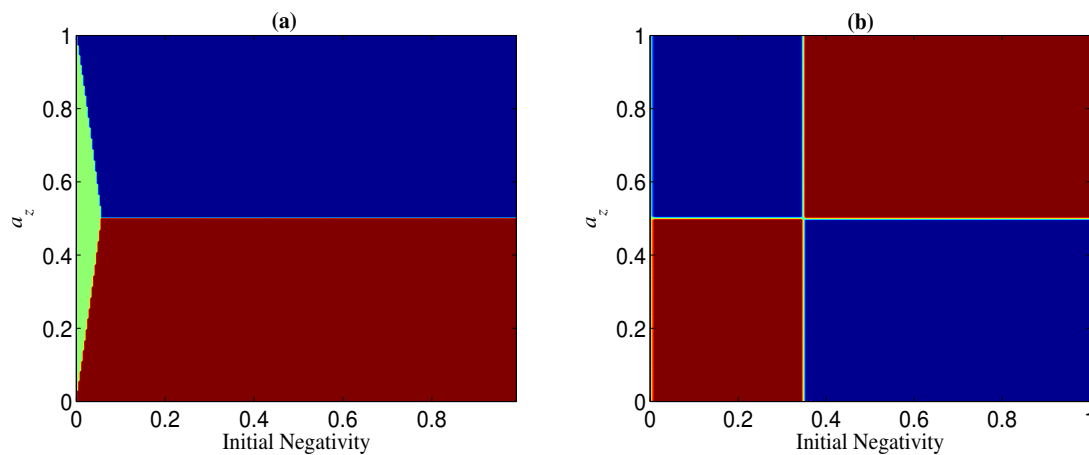


Figure 14. Regions of $\Delta\mathcal{N} < 0$ (blue), $\Delta\mathcal{N} > 0$ (red), and $\Delta\mathcal{N} = 0$ (green) when $a_y = 0$ and $p = 0.1$. (a) $n = 2$; (b) $n = 3$.

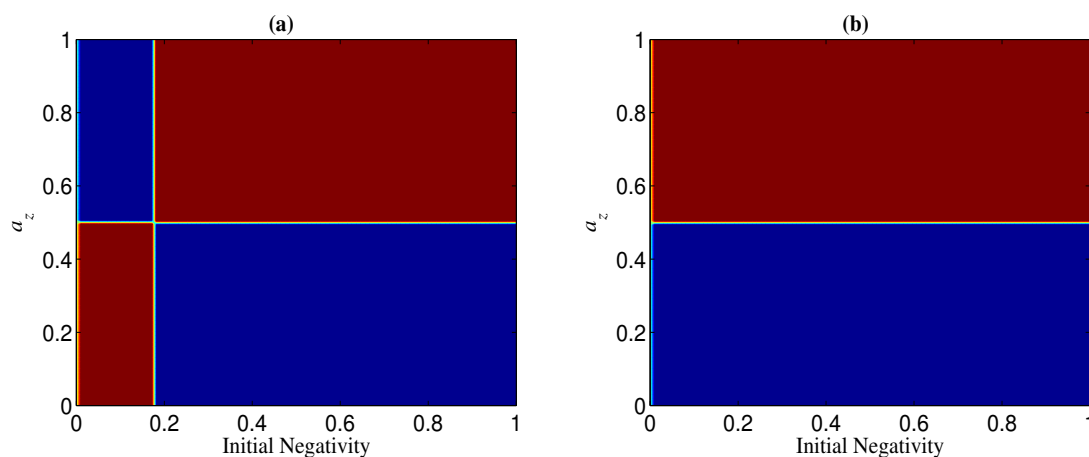


Figure 15. Regions of $\Delta\mathcal{N} < 0$ (blue) and $\Delta\mathcal{N} > 0$ (red) when $a_y = 0$ and $p = 0.1$. (a) $n = 4$; (b) $n = 25$.

3. Conclusions

In summary, we investigated the decoherence features and entanglement-robustness of cat-like states in the local Pauli noises where the probabilities of three kinds of errors occurring are not the

same. It was shown that the decay law of a cat-like state is not only related to the overall noise strength (p), but also to the error distribution parameters (a_x, a_y, a_z), and that the robustness of both two-qubit and multi-qubit states in a given noisy environment is dependent on the basis of qubits. Whether a two-qubit entangled state is more robust in the computational basis $\{|0\rangle, |1\rangle\}$ or transversal basis $\{|+\rangle, |-\rangle\}$ only depends on the error distribution parameters. Specifically, in terms of the entanglement-robustness of two-qubit states, the basis $\{|+\rangle, |-\rangle\}$ is superior to $\{|0\rangle, |1\rangle\}$ when $a_z < (1 - a_y)/2$ and $\{|0\rangle, |1\rangle\}$ is superior to $\{|+\rangle, |-\rangle\}$ when $a_z > (1 - a_y)/2$. However, which basis can be used to enhance the entanglement-robustness of multi-qubit states is not only dependent on the error distribution parameters, but also on the overall noise strength, the initial degree of entanglement, and the number of qubits. In other words, the better basis for a multi-qubit state may be not the same in different noisy environments, and the better basis for two multi-qubit states may be different in the same noisy environment. These phenomena also lead to another interesting result that the better basis for a two-qubit state and a multi-qubit state with the same degree of bipartite entanglement may be different. That is to say, if a two-qubit state is more robust under the basis $\{|0\rangle, |1\rangle\}$, a multi-qubit state with the same amount of bipartite entanglement may be more robust under the basis $\{|+\rangle, |-\rangle\}$. In addition, an M -qubit cat-like state could be more robust than a L -qubit ($M > L$) cat-like state having the same superposition coefficients with the former under the same qubit basis, although each qubit suffers from a Pauli noise.

The aforementioned results tell us that one could improve the robustness of cat-like entangled states in local Pauli noises by simply transforming the qubit basis. In some scenarios, one can change the basis, according to preestimated channel features, before the qubits undergoing decoherence. In other scenarios, it may be necessary to change the basis during the process of decoherence. Practically, when we should transform the basis depends on the fact of whether the better basis is related to the noise strength p characterizing the decoherence time. This enhancement method is much simpler and more efficient than the others because it does not introduce extra particles and works in a deterministic manner. Due to the inherent relationship between quantum entanglement and quantum coherence [57], it may be interesting to investigate whether or how the basis rotation could contribute to the preservation of quantum coherence that has attracted attention recently [58,59].

Author Contributions: X.-W.W. put forward the original idea, contributed to all aspects of this study, and wrote the manuscript. S.-Q.T., Y.L., and J.-B.Y. contributed equally to the calculation and analysis of some results, and the revisions of the manuscript.

Funding: This work was supported by the NSFC (Grant No. 11847010), the Scientific Research Fund of Hunan Provincial Education Department (Grant No. 15A028 and No. 16B036), the HNNSF (Grant No. 2017JJ3005), the Science and Technology Plan Project of Hunan Province (Grant No. 2016TP1020), the Open Fund Project of Hunan Provincial Key Laboratory of Intelligent Information Processing and Application for Hengyang Normal University (Grant No. IIPA18K07), the Hunan Provincial Applied Basic Research Base of Optoelectronic Information Technology (Grant No. GD18K03), and the Open Fund of Key Laboratory of Low-Dimensional Quantum Structures and Quantum Control of Ministry of Education (Grant No. QSQC1702).

Conflicts of Interest: The authors declare no conflict of interest.

Appendix A

For convenience, we define notations $\mathbf{j} = j_1 j_2 \cdots j_n$ and $\bar{\mathbf{j}} = \bar{j}_1 \bar{j}_2 \cdots \bar{j}_n$, where $j_m \in \{0, 1\}$ and $\bar{j}_m = 1 - j_m$ ($m = 1, 2, \cdots, n$). Under the basis $\{|\mathbf{j}\rangle, \mathbf{j} = \mathbf{0}, \cdots, \mathbf{1}\}$, the decohered state $\mathcal{M}(|\Phi_n^+\rangle)$ can be denoted by a X matrix ϱ with diagonal and anti-diagonal elements

$$\varrho_{\mathbf{j}, \mathbf{j}} = A^{n-|\mathbf{j}|} B^{|\mathbf{j}|} \alpha^2 + A^{|\mathbf{j}|} B^{n-|\mathbf{j}|} \beta^2, \quad (\text{A1})$$

$$\varrho_{\mathbf{j}, \bar{\mathbf{j}}} = \left(C^{n-|\mathbf{j}|} D^{|\mathbf{j}|} + C^{|\mathbf{j}|} D^{n-|\mathbf{j}|} \right) \alpha \beta, \quad (\text{A2})$$

where $|\mathbf{j}|$ denotes the number of “one” in the bit string \mathbf{j} , e.g., $|\mathbf{0}\rangle = 0$ and $|\mathbf{1}\rangle = n$. A, B, C, D are defined in Equations (11)–(14), respectively. Without loss of generality, we consider the bipartition “qubit one versus the rest”, and introduce a notation $\mathbf{j} = j_1 \mathbf{j}'$ with $\mathbf{j}' = j_2 j_3 \cdots j_n$. Then, the elements of

the partial transpose ϱ^T of ϱ are $\varrho_{j_1 j', j_1 j'}^T = \varrho_{j_1 j', j_1 j'}$ and $\varrho_{j_1 j', j_1 \bar{j}'}^T = \varrho_{j_1 j', j_1 \bar{j}'}$. Calculation of the eigenvalues of the $2^n \times 2^n$ -dimensional X matrix ϱ^T is essentially equivalent to diagonalizing 2^{n-1} matrices of dimension 2×2 , given by

$$\begin{pmatrix} \varrho_{0j',0j'} & \varrho_{1j',0\bar{j}'} \\ \varrho_{0\bar{j}',1j'} & \varrho_{1\bar{j}',1\bar{j}'} \end{pmatrix} \tag{A3}$$

with $|j'|$ ranging from 0 to $n - 1$. The eigenvalues of these 2×2 -dimensional matrices are given by

$$\lambda_{\pm}^{|j'|} = \frac{1}{2} (\varrho_{0j',0j'} + \varrho_{1\bar{j}',1\bar{j}'}) \pm \frac{1}{2} \sqrt{(\varrho_{0j',0j'} - \varrho_{1\bar{j}',1\bar{j}'})^2 + 4\varrho_{1j',0\bar{j}'}\varrho_{0\bar{j}',1j'}}. \tag{A4}$$

It can be directly calculated that

$$\varrho_{0j',0j'} + \varrho_{1\bar{j}',1\bar{j}'} = A^{|j'|} B^{n-|j'|} + A^{n-|j'|} B^{|j'|}, \tag{A5}$$

$$\varrho_{0j',0j'} - \varrho_{1\bar{j}',1\bar{j}'} = (A^{n-|j'|} B^{|j'|} - A^{|j'|} B^{n-|j'|}) \sqrt{1 - \mathcal{N}_i^2}, \tag{A6}$$

$$4\varrho_{1j',0\bar{j}'}\varrho_{0\bar{j}',1j'} = (C^{n-1-|j'|} D^{1+|j'|} + C^{1+|j'|} D^{n-1-|j'|})^2 \mathcal{N}_i^2, \tag{A7}$$

where identity $|j'| + |\bar{j}'| = n - 1$ has been used. Using the definition of negativity given in Equation (3), we have

$$\begin{aligned} \mathcal{N} &= \sum_{|j'|=0}^{n-1} \binom{n-1}{|j'|} \max(0, -2\lambda_-^{|j'|}) \\ &= \sum_{|j'|=0}^{\lfloor \frac{n-1}{2} \rfloor} \binom{n-1}{|j'|} \max(0, -2\lambda_-^{|j'|}) + \sum_{|j'|=\lfloor \frac{n-1}{2} \rfloor+1}^{n-1} \binom{n-1}{|j'|} \max(0, -2\lambda_-^{|j'|}) \\ &= \sum_{u=0}^{\lfloor \frac{n-1}{2} \rfloor} \binom{n-1}{u} \max(0, H_u - F_u) + \sum_{u=0}^{\lfloor \frac{n-1}{2} \rfloor} \binom{n-1}{u} \max(0, G_u - F_{u+1}), \end{aligned} \tag{A8}$$

where $\lfloor \frac{n-1}{2} \rfloor = (n - 1)/2$, for n being odd, or $\lfloor \frac{n-1}{2} \rfloor = n/2 - 1$, for n being even, and F_u, G_u, H_u are defined in Equations (8)–(10), respectively.

References

- Nielsen, M.A.; Chuang, I.L. *Quantum Computation and Quantum Information*; Cambridge University Press: Cambridge, UK, 2000.
- Brunner, N.; Cavalcanti, D.; Pironio, S.; Scarani, V.; Wehner, S. Bell nonlocality. *Rev. Mod. Phys.* **2014**, *86*, 419–478. [[CrossRef](#)]
- Vedral, V. Quantum entanglement. *Nat. Phys.* **2014**, *10*, 256–258. [[CrossRef](#)]
- Lo Franco, R.; Compagno, G. Quantum entanglement of identical particles by standard information-theoretic notions. *Sci. Rep.* **2016**, *6*, 20603. [[CrossRef](#)] [[PubMed](#)]
- Pan, J.W.; Chen, Z.B.; Lu, C.Y.; et al. Multiphoton entanglement and interferometry. *Rev. Mod. Phys.* **2012**, *84*, 777–838. [[CrossRef](#)]
- Lo Franco, R.; Compagno, G. Indistinguishability of Elementary Systems as a Resource for Quantum Information Processing. *Phys. Rev. Lett.* **2018**, *120*, 240403. [[CrossRef](#)] [[PubMed](#)]
- Rab, A.S.; Polino, E.; Man, Z.X.; An, N.B.; Xia, Y.-J.; Spagnolo, N.; Franco, R.L.; Sciarrino, F. Entanglement of photons in their dual wave-particle nature. *Nat. Commun.* **2017**, *8*, 915. [[CrossRef](#)] [[PubMed](#)]
- Gardiner, C.W.; Zoller, P. *Quantum Noise*, 3rd ed; Springer: Berlin, Germany, 2004.
- Aolita, L.; de Melo, F.; Davidovich, L. Open-system dynamics of entanglement: A key issues review. *Rep. Prog. Phys.* **2015**, *78*, 042001. [[CrossRef](#)]

10. Knoll, L.T.; Schmiegelow, C.T.; Larotonda, M.A. Noisy quantum teleportation: An experimental study on the influence of local environments. *Phys. Rev. A* **2014**, *90*, 042332. [[CrossRef](#)]
11. Cavalcanti, D.; Skrzypczyk, P.; Šupić, I. All Entangled States can Demonstrate Nonclassical Teleportation. *Phys. Rev. Lett.* **2017**, *119*, 110501. [[CrossRef](#)]
12. Chaves, R.; Brask, J.B.; Markiewicz, M.; Kołodyński, J.; Acín, A. Noisy Metrology beyond the Standard Quantum Limit. *Phys. Rev. Lett.* **2013**, *111*, 120401. [[CrossRef](#)]
13. Horodecki, R.; Horodecki, P.; Horodecki, M.; Horodecki, K. Quantum entanglement. *Rev. Mod. Phys.* **2009**, *81*, 865–942. [[CrossRef](#)]
14. Duan, L.M.; Monroe, C. Quantum networks with trapped ions. *Rev. Mod. Phys.* **2010**, *82*, 1209–1224. [[CrossRef](#)]
15. Carvalho, A.R.R.; Santos, M.F. Distant entanglement protected through artificially increased local temperature. *New J. Phys.* **2011**, *13*, 013010. [[CrossRef](#)]
16. Mascarenhas, E.; Cavalcanti, D.; Vedral, V.; Santos, M.F. Physically realizable entanglement by local continuous measurements. *Phys. Rev. A* **2011**, *83*, 022311. [[CrossRef](#)]
17. Hartmann, L.; Dür, W.; Briegel, H.J. Steady-state entanglement in open and noisy quantum systems. *Phys. Rev. A* **2006**, *74*, 052304. [[CrossRef](#)]
18. Carvalho, A.R.R.; Reid, A.J.S.; Hope, J.J. Controlling entanglement by direct quantum feedback. *Phys. Rev. A* **2008**, *78*, 012334. [[CrossRef](#)]
19. Platzer, F.; Mintert, F.; Buchleitner, A. Optimal dynamical control of many-body entanglement. *Phys. Rev. Lett.* **2010**, *105*, 020501. [[CrossRef](#)]
20. Sun, Q.; Al-Amri, M.; Davidovich, L.; Zubairy, M. Reversing entanglement change by a weak measurement. *Phys. Rev. A* **2010**, *82*, 052323. [[CrossRef](#)]
21. Kim, Y.S.; Lee, J.C.; Kwon, O.; Kim, Y.H. Protecting entanglement from decoherence using weak measurement and quantum measurement reversal. *Nat. Phys.* **2012**, *8*, 117–120. [[CrossRef](#)]
22. Xu, J.S.; Sun, K.; Li, C.F.; Xu, X.; Guo, G.; Andersson, E.; Franco, R.L.; Compagno, G. Experimental recovery of quantum correlations in absence of system–environment back-action. *Nat. Commun.* **2013**, *4*, 2851. [[CrossRef](#)]
23. Lo Franco, R.; D’Arrigo, A.; Falci, G.; Compagno, G.; Paladino, E. Preserving entanglement and nonlocality in solid-state qubits by dynamical decoupling. *Phys. Rev. B* **2014**, *90*, 054304. [[CrossRef](#)]
24. D’Arrigo, A.; Lo Franco, R.; Benenti, G.; Paladino, E.; Falci, G. Recovering entanglement by local operations. *Ann. Phys.* **2014**, *350*, 211–224. [[CrossRef](#)]
25. Terhal, B.M. Quantum error correction for quantum memories. *Rev. Mod. Phys.* **2015**, *87*, 307–346. [[CrossRef](#)]
26. Orioux, A.; D’Arrigo, A.; Ferranti, G.; Paladino, E.; Falci, G.; Sciarrino, F.; Mataloni, P. Experimental on-demand recovery of entanglement by local operations within non-Markovian dynamics. *Sci. Rep.* **2015**, *5*, 8575. [[CrossRef](#)] [[PubMed](#)]
27. D’Arrigo, A.; Benenti, G.; Lo Franco, R.; Falci, G.; Paladino, E. Hidden entanglement, system–environment information flow and non-Markovianity. *Int. J. Quantum Inf.* **2014**, *12*, 1461005. [[CrossRef](#)]
28. Man, Z.X.; Xia, Y.J.; Lo Franco, R. Cavity-based architecture to preserve quantum coherence and entanglement. *Sci. Rep.* **2015**, *5*, 13843. [[CrossRef](#)] [[PubMed](#)]
29. Ong, E.T.S.; Chew, L.Y. The Effect of Spin Squeezing on the Entanglement Entropy of Kicked Tops. *Entropy* **2016**, *18*, 116. [[CrossRef](#)]
30. Lo Franco, R. Nonlocality threshold for entanglement under general dephasing evolutions: A case study. *Quantum Inf. Process.* **2016**, *15*, 2393–2404. [[CrossRef](#)]
31. Morteza pour, A.; Naeimi, G.; Lo Franco, R. Coherence and entanglement dynamics of vibrating qubits. *Opt. Commun.* **2018**, *424*, 26–31. [[CrossRef](#)]
32. Morteza pour, A.; Lo Franco, R. Protecting quantum resources via frequency modulation of qubits in leaky cavities. *Sci. Rep.* **2018**, *8*, 14304. [[CrossRef](#)]
33. Bennett, C.H.; DiVincenzo, D.P.; Smolin, J.A.; Wootters, W.K. Mixed state entanglement and quantum error correction. *Phys. Rev. A* **1996**, *54*, 3824–3851. [[CrossRef](#)] [[PubMed](#)]
34. Bennett, C.H.; Brassard, G.; Popescu, S.; Smolin, J.A.; Wootters, W.K. Purification of Noisy Entanglement and Faithful Teleportation via Noisy Channels. *Phys. Rev. Lett.* **1996**, *76*, 722–725. [[CrossRef](#)] [[PubMed](#)]
35. Murao, M.; Plenio, M.B.; Popescu, S.; Vedral, V.; Knight, P.L. Multiparticle entanglement purification protocols. *Phys. Rev. A* **1998**, *57*, R4075–R4078. [[CrossRef](#)]
36. Aschauer, H.; Dür, W.; Briegel, H.J. Multiparticle entanglement purification for two-colorable graph states. *Phys. Rev. A* **2005**, *71*, 012319. [[CrossRef](#)]

37. Czechlewski, M.; Grudka, A.; Ishizaka, S.; Wójcik, A. Entanglement purification protocol for a mixture of a pure entangled state and a pure product state. *Phys. Rev. A* **2009**, *80*, 014303. [[CrossRef](#)]
38. Wang, X.W.; Tang, S.Q.; Yuan, J.B.; Zhang, D.Y. Distilling perfect GHZ states from two copies of non-GHZ-diagonal mixed states. *Opt. Commun.* **2017**, *392*, 185–189. [[CrossRef](#)]
39. Yuan, J.; Tang, S.; Wang, X.; Zhang, D. One-step distillation of local-unitary-equivalent GHZ-type states. *Quantum Inf. Process.* **2018**, *17*, 259. [[CrossRef](#)]
40. Horodecki, M.; Horodecki, P.; Horodecki, R. Inseparable two spin-1/2 density matrices can be distilled to a singlet form. *Phys. Rev. Lett.* **1997**, *78*, 574–577. [[CrossRef](#)]
41. Kwiat, P.G.; Barraza-Lopez, S.; Stefanov, A.; Gisin, N. Experimental entanglement distillation and ‘hidden’ non-locality. *Nature* **2001**, *409*, 1014–1017. [[CrossRef](#)]
42. Wang, X.W.; Yu, S.; Zhang, D.Y.; Oh, C.H. Effect of weak measurement on entanglement distribution over noisy channels. *Sci. Rep.* **2016**, *6*, 22408. [[CrossRef](#)]
43. Fröwis, F.; Dür, W. Stability of encoded macroscopic quantum superpositions. *Phys. Rev. A* **2012**, *85*, 052329. [[CrossRef](#)]
44. Filippov, S.N.; Frizen, V.V.; Kolobova, D.V. Ultimate entanglement robustness of two-qubit states against general local noises. *Phys. Rev. A* **2018**, *97*, 012322. [[CrossRef](#)]
45. Mintert, F. Robust entangled states. *J. Phys. A Math. Theor.* **2010**, *43*, 245303. [[CrossRef](#)]
46. Yu, T.; Eberly, J.H. Evolution from entanglement to decoherence of bipartite mixed “X” states. *Quantum Inf. Comput.* **2007**, *7*, 459–468.
47. Chaves, R.; Aolita, L.; Acín, A. Robust multipartite quantum correlations without complex encodings. *Phys. Rev. A* **2012**, *86*, 020301(R). [[CrossRef](#)]
48. Ali, M.; Gühne, O. Robustness of multiparticle entanglement: Specific entanglement classes and random states. *J. Phys. B At. Mol. Opt. Phys.* **2014**, *47*, 055503. [[CrossRef](#)]
49. Arthur, T.T.; Martin, T.; Fai, L.C. Disentanglement and quantum states transitions dynamics in spin-qutrit systems: Dephasing random telegraph noise and the relevance of the initial state. *Quantum Inf. Process.* **2018**, *17*, 37. [[CrossRef](#)]
50. Aolita, L.; Cavalcanti, D.; Chaves, R.; Dhara, C.; Davidovich, L.; Acin, A. Noisy evolution of graph-state entanglement. *Phys. Rev. A* **2010**, *82*, 032317. [[CrossRef](#)]
51. Shen, L.T.; Shi, Z.C.; Wu, H.Z.; Yang, Z.B. Dynamics of Entanglement in Jaynes-Cummings Nodes with Nonidentical Qubit-Field Coupling Strengths. *Entropy* **2017**, *19*, 331. [[CrossRef](#)]
52. Borrás, A.; Majtey, A.P.; Plastino, A.R. Robustness of highly entangled multiqubit states under decoherence. *Phys. Rev. A* **2009**, *79*, 022108. [[CrossRef](#)]
53. Kesting, F.; Fröwis, F.; Dür, W. Effective noise channels for encoded quantum systems. *Phys. Rev. A* **2013**, *88*, 042305. [[CrossRef](#)]
54. Vidal, G.; Werner, R.F. Computable measure of entanglement. *Phys. Rev. A* **2002**, *65*, 032314. [[CrossRef](#)]
55. Życzkowski, K.; Horodecki, P.; Sanpera, A.; Lewenstein, M. Volume of the set of separable states. *Phys. Rev. A* **1998**, *58*, 883–892. [[CrossRef](#)]
56. Hashemi Rafsanjani, S.M.; Huber, M.; Broadbent, C.J.; Eberly, J.H. Genuinely multipartite concurrence of N-qubit X matrices. *Phys. Rev. A* **2012**, *86*, 062303. [[CrossRef](#)]
57. Streltsov, A.; Adesso, G.; Plenio, M.B. Quantum coherence as a resource. *Rev. Mod. Phys.* **2017**, *89*, 041003. [[CrossRef](#)]
58. Bromley, T.R.; Cianciaruso, M.; Adesso, G. Frozen Quantum Coherence. *Phys. Rev. Lett.* **2015**, *114*, 210401. [[CrossRef](#)] [[PubMed](#)]
59. Silva, I.A.; Souza, A.M.; Bromley, T.R.; Cianciaruso, M.; Marx, R.; Sarthour, R.S.; Oliveira, I.S.; Franco, R.L.; Glaser, S.J.; deAzevedo, E.R.; et al. Observation of Time-Invariant Coherence in a Nuclear Magnetic Resonance Quantum Simulator. *Phys. Rev. Lett.* **2016**, *117*, 160402. [[CrossRef](#)] [[PubMed](#)]

